PCCP

PAPER

View Article Online
View Journal | View Issue



Cite this: *Phys. Chem. Chem. Phys.*, 2025, **27**, 4663

# Insights into the mechanism of electrochemical chloride oxidation in ethanol from X-ray photoelectron spectroscopy, quiescent solution voltammetry, and rotating ring-disk electrodes†

Ryan D. Van Daele, ‡ Siqi Li, ‡ Katherine H. Morrissey and Bart M. Bartlett *

Received 17th June 2024,
Accepted 30th January 2025

DOI: 10.1039/d4cp02429j

rsc.li/pccp

The wide availability of bio-derived alcohols provides the impetus to develop processes that convert them to valuable chemicals. The chloride ion is a redox mediator for electrocatalytic ethanol oxidation to 1,1-diethoxyethane (1,1-DEE) through an ethyl hypochlorite (EtOCl) intermediate, and this paper describes the chloride oxidation reaction (COR) to EtOCl on a glassy carbon (GC) electrode. Voltammetry measurements on a GC electrode in inert acetonitrile solvent combined with *ex situ* X-ray photoelectron spectroscopy (XPS) establish a Volmer step, where chloride ion from solution chemisorbs and is oxidized. In reactive ethanol solvent, ethanol adsorbs, and analyzing the current response in an LSV experiment supports a two-electron-transfer to form EtOCl, with chemisorption of the regenerated chloride. Koutecký–Levich (K–L) analysis on a rotating ring disk electrode (RRDE) shows that the kinetic rate constant of the COR in ethanol is on the order of $10^{-8}$ cm $s^{-1}$, which is five orders of magnitude faster than the direct alcohol oxidation reaction in a kinetically limited regime. This hydrodynamic approach in understanding the electrochemistry of this non-aqueous system extends the possibilities for mediated electrocatalysis in neat alcohol solvents.



## Introduction

Electrochemical synthesis, functionalization, and transformations of organic molecules have seen a renaissance in recent years, spurred by an emphasis on green chemistry and insights from energy-relevant catalytic reactions. Oxidation and reduction occur by electron transfer reactions on electrodes rather than through stoichiometric chemical reagents.[1] With developments in photovoltaic and photoelectrochemical approaches, electrochemical synthesis also allows renewable energy inputs from solar irradiation.[2,3] In terms of substrates, small-molecule alcohols can be produced from biomass feedstocks from agricultural practices, exemplified in the well-established biorefinery industry, with a global annual production of $10^{10}$ gallons of ethanol.[4] Moreover, selective alcohol oxidation yields a range of industrially-relevant products including aldehydes, carboxylic acids, esters, and even polymers.[5] Bioderived precursors provide an alternative towards petrochemistry, which relies on the cracking of crude oil.[6] The vast availability of bioethanol also presents the potential to power next-generation fuel cells, direct alcohol fuel cells (DAFCs), once an appropriate electrocatalyst is identified.[7]

Mediated electrocatalysis is a critical approach employed to accelerate the reaction rates and to enhance control over mechanistic pathways to direct forming a specific product. In oxidation reactions (as will be the subject of this paper), the solution-phase mediator diffuses to the anode, electron transfer takes place, and the oxidized intermediate diffuses away. These steps are rapid, and the oxidized form of the mediator carries out substrate oxidation as a solution chemical step away from the electrode. This approach not only circumvents the slow mass transport and adsorption/desorption of large organic substrates, but also prevents direct electron transfer between the substrate and the anode that could result in poor selectivity due to passivation of the working electrode by the product and/or intermediates.[8,9]

In the field of mediated electrocatalysis, *N*-oxyl radicals such as TEMPO are the most sought after due to their rapid, reversible kinetics.[10,11] This couple is often used on a glassy carbon electrode, as used in this manuscript. However, for the purpose of larger scale practices, the search for non-toxic, low-cost inorganic mediators remains critical and is unfortunately not yet as well established. Our research group has demonstrated using the nitrate ($NO_3^-$/$NO_3^\bullet$) couple on platinum electrodes and the chloride ($Cl^-$/HClO) couple on tungsten oxide photoelectrodes to affect selective alcohol oxidation chemistry.[12,13] We find that in

*Department of Chemistry, University of Michigan 930 N. University Avenue, Ann Arbor, Michigan, 48109-1055, USA. E-mail: bartmb@umich.edu*

† Electronic supplementary information (ESI) available. See DOI: https://doi.org/10.1039/d4cp02429j

‡ R. D. V. D. and S. L. contributed equally to this work.

electrochemical reactions, the nitrate couple leads to H-atom abstraction from acetonitrile solvent. This parasitic reaction irreversibly consumes nitrate.[14] Most recently, we discovered that chloride-mediated ethanol oxidation on glassy carbon can be carried out electrochemically with no additional solvent, selectively yielding 1,1-diethoxyethane (DEE) as the 2-electron oxidation product with >95% faradaic efficiency by producing an ethyl hypochlorite (EtOCl) intermediate.[15] It is noteworthy that in this work, EtOCl neither serves as a direct oxidant nor carries out functionalization (by transferring chlorine), and the product forms due to its spontaneous decomposition. However, alkyl hypochlorites could indeed act as oxidants, providing the impetus of studying their reactivity through RRDE methods.[16]

There are a couple of other examples of mediated catalysis for neat ethanol oxidation on glassy carbon electrodes. One example is using ruthenium isoindolines with added hydroxide, where the $Ru^{4+/2+}$ couple engenders ethanol oxidation to acetaldehyde, ethyl acetate and 1,1-DEE.[17] Similarly, researchers optimized the system towards a bimetallic Ru–Pt complex for methanol oxidation to methyl formate and 1,1-dimethoxymethane.[18] Using chloride as the mediator in neat alcohol not only provides higher current density and better selectivity than what is reported in these cases, but is also far more abundant and much less toxic compared to the noble metal reagents.

This work contrasts the aqueous redox chemistry of chlorine. Depending on the pH, chloride oxidation may produce $Cl_2$, HClO, or $ClO^-$, and the corresponding electrochemical pathways have been well established.[19,20] Another recent work on chloride-mediated ethanol conversion in aqueous conditions highlights the electrochemical generation of chlorine radicals, that selectively attack either the α or β hydrogens, resulting in either acetic acid or ethylene oxide as the product.[21] Chloride oxidation in neat ethanol yields only EtOCl as the intermediate, hinting that the reaction proceeds through a different mechanism. In this paper, we combine voltammetry, surface characterization by X-ray photoelectron spectroscopy (XPS), hydrodynamic kinetics experiments using rotating ring-disk electrodes (RRDEs), and *in situ* spectroelectrochemistry to substantiate this reaction mechanism.

## Results and discussion

The catalytic reaction of ultimate interest is chloride consumption and regeneration (*i.e.* – chloride-mediated) ethanol oxidation:

$$Cl^- + CH_3CH_2OH \rightarrow CH_3CH_2OCl + H^+ + 2e^- \quad (1)$$

$$CH_3CH_2OCl \rightarrow CH_3CHO + H^+ + Cl^- \quad (2)$$

The first reaction is electrochemical, formally oxidizing the chloride ion by two electrons. The second reaction is purely chemical, the decomposition of EtOCl, to form acetaldehyde and regenerate the chloride ion. This two-step process allows for oxidation at lower applied bias than that required for the direct electrochemical ethanol oxidation reaction:

$$CH_3CH_2OH \rightarrow CH_3CHO + 2H^+ + 2e^- \quad (3)$$

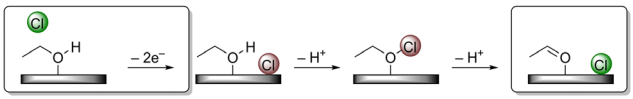


Scheme 1 Proposed mechanism of the chloride oxidation reaction in neat ethanol on a GC electrode. The steps in the boxes are observable. Green and red spheres for chlorine represent $Cl^-$ and $Cl^+$, respectively.

Previous work focused on the kinetics of the chemical step (eqn (2)), and that rate constant is $7 \times 10^{-4}$ $s^{-1}$.[15] Here we focus on the electrochemical steps required for eqn (1). Based on XPS analysis and several electrochemical measurements, we propose that the net two-electron chloride oxidation reaction (COR) in neat ethanol on glassy carbon (GC) electrodes proceeds by forming a two-electron oxidized chloronium-like species, formally $Cl^+$, as is typically invoked in the chlorine-evolution reaction in water,[22] that reacts rapidly with ethanol solvent to form the EtOCl intermediate, illustrated in Scheme 1. Notably, GC electrodes have been shown to facilitate such inner-sphere electron-transfer reactions.[23] Descriptions and photographs of all the electrochemistry experimental setups are presented in the electronic ESI† (Fig. S1–S5).

### 1. XPS evidence for chlorine chemisorption on glassy carbon

The first question we wanted to answer is what species adsorb to the glassy carbon electrode in chloride-containing solution? To answer this, we conducted X-ray photoelectron spectroscopy (XPS) measurements on a series of GC electrodes. We started by comparing the chlorine $^2P$ lines (2p core excitation) and carbon $^2S$ lines (1s core excitation) for a GC electrode that is merely soaked in chloride, ethanol, and supporting $Bu_4NOTf$ electrolyte *versus* one that is polarized to +1.9 V *vs.* $Fc^{+/0}$ in a linear sweep voltammetry (LSV) sweep starting at open circuit (0.2 V *vs.* $Fc^{+/0}$) with a scan rate of 1 mV $s^{-1}$ to carry out the COR. In this scan (Fig. 1a), peak anodic current, $i_{pa}$ appears at 1.49 V *vs.*

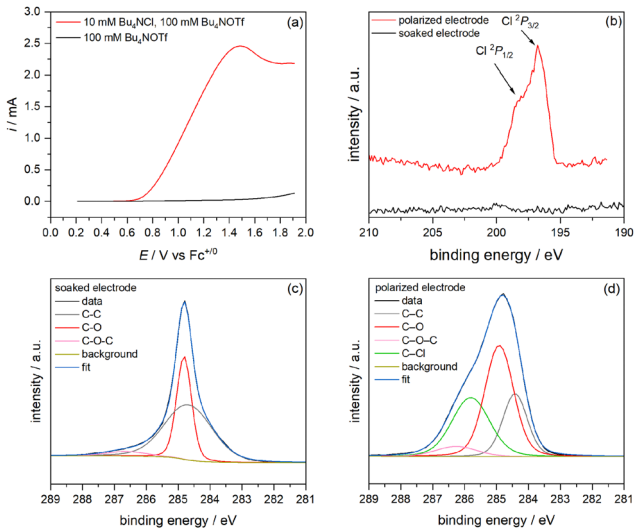


Fig. 1 (a) LSV sweep of 10 mM $Bu_4NCl$ in ethanol. The scan rate is 1 mV $s^{-1}$; XPS data on GC electrodes. (b) Cl 2p after soaking or polarizing in $Bu_4NCl$ in ethanol solvent; (c) C 1s after soaking; (d) C 1s after polarizing.

$Fc^{+/0}$, and the duration of this experiment was ~35 minutes. After the COR, the GC plate was rinsed three times with ethanol to remove any excess electrolyte or physisorbed chloride before transferring the sample to an air-free XPS sample holder. In the control soaking experiment, GC was immersed in chloride solution for 35 minutes as well. The XPS data in Fig. 1b show that nothing sticks by merely soaking GC in chloride solution, but after polarizing the electrode, chlorine lines appear at 198.3 eV and 196.7 eV for $^2P_{1/2}$ and $^2P_{3/2}$, respectively. These binding energies are slightly lower in energy than the reference values for typical inorganic chloride ions, 201 and 199.[24] This approximately 2.5 eV difference is likely due to the differences that arise in assigning the adventitious carbon binding energy peak, since the GC surface also changes (*vide infra*).

The carbon 1s spectrum in Fig. 1c for the film soaked in 10 mM $Bu_4NCl$ and 100 mM $Bu_4NOTf$ for 35 minutes gives a carbon envelope that was fit with 3 binding environments with C–C bonding, C–O bonding, and C–O–C bonding, which we hypothesize to be ethanol at the surface based on comparable reported literature values (286.2 eV).[25] The binding energies and relative peak areas of each bonding environment are provided in Table 1. Fig. 1d shows that when the electrode is poised to positive potential to carry out the COR, a C–Cl feature appears at 285.8 eV. Moreover, the relative area of the C–O bonding envelope increases as the oxidized product is formed.

We know from our previous work that an EtOCl intermediate is formed (formally $Cl^+$), but we do not directly observe any oxidized chlorine species in ethanol, likely because its reaction with the solvent is fast. So, to establish that chloride is oxidized and chemisorbs to GC, we repeated the electrochemistry and subsequent XPS experiments in acetonitrile, where chloride ion is the only electrochemically active (oxidizable) species with no other reactant for a subsequent chemical step. Fig. 2a shows the LSV trace recorded in an argon glove box, starting at open circuit and sweeping in the positive direction to 0.7 V *vs.* $Fc^{+/0}$ at a scan rate of 1 mV $s^{-1}$. After this electrochemical oxidation, the GC plate was rinsed three times with solvent to remove any excess physisorbed electrolyte and solvent before transferring the electrode to the air-free XPS sample holder. Fig. 2b shows two distinct chlorine $^2P$ lines. The lower binding energy lines at 199 eV and 198 eV for $^2P_{1/2}$ and $^2P_{3/2}$, respectively, closely match the reference values for chloride ion, $Cl^-$.[26] However, the pair of peaks with higher binding energies, 203 eV and 201 eV, is consistent with chemisorbed $Cl^0$, the product of a Volmer step.[26,27] Although the binding energies of a formal $Cl^+$ species are not established, the observation of oxidized chlorine in this experiment stands in support of the mechanism proposed in Scheme 1. Fitting these XPS lines is complicated by the overlap of the phosphorus $^2S$ line from the $PF_6^-$ electrolyte used in this experiment, but further evidence for C–Cl bonding comes from the carbon 1s envelope, where a peak grows in at 287.3 eV (Fig. S6, ESI†).

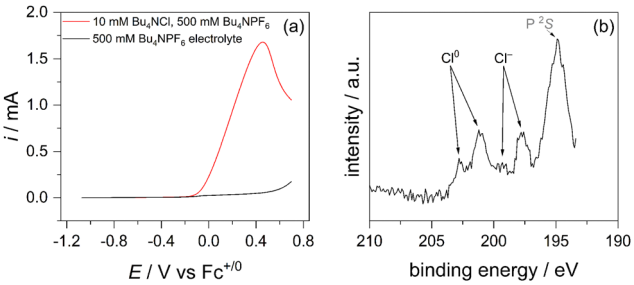


Fig. 2 (a) LSV traces from OCP to 0.7 V *vs.* $Fc^{0/+}$ with 10 mM $Bu_4NCl$ (red) and without (black) chloride in 500 mM $Bu_4NPF_6$ supporting electrolyte; (b) Cl 2p XPS of the GC carbon electrode after the LSV experiment showing both $Cl^-$ and oxidized $Cl^0$.

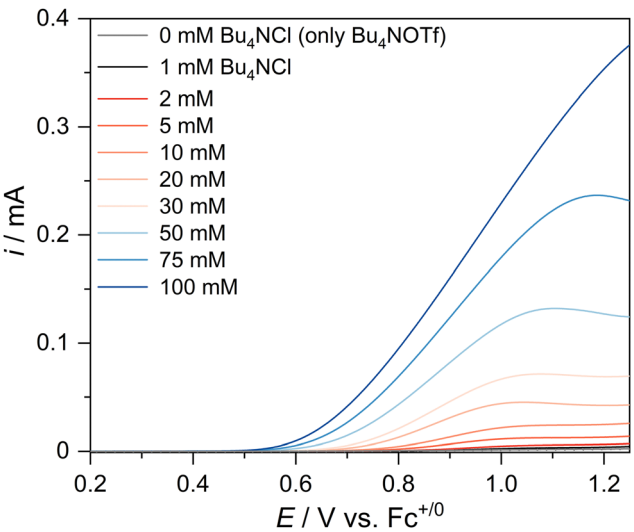


Fig. 3 LSV curves on a GC disk in solutions of varying chloride concentration. The scan rate is 5 mV $s^{-1}$. The control experiment with no chloride is also included (gray) for comparison.

## 2. Voltammetry measurements in quiescent solutions show two-electron chemistry on GC

In this section, we establish that the chloride ion in solution is the electrochemically active substrate, and we answer the questions: over what range of chloride concentration do see current that is limited by reaction kinetics and how many electrons transfer? We carried out LSV experiments in quiescent solutions with varying chloride concentrations. Here, a 200 mM ionic strength was maintained by adding $Bu_4NOTf$, as described in the last section. Fig. 3 shows the LSV curves in

Table 1 Carbon 1s XPS data on GC electrodes in chloride electrolyte and ethanol solvent

| History | $BE_{C-C}$/eV | $Area_{C-C}$ | $BE_{C-O}$/eV | $Area_{C-O}$ | $BE_{C-O-C}$/eV | $Area_{C-O-C}$ | $BE_{C-Cl}$/eV | $Area_{C-Cl}$ |
|---|---|---|---|---|---|---|---|---|
| Soaked | 284.7 | 0.6026 | 284.8 | 0.3548 | 286.6 | 0.0426 | — | — |
| Polarized | 284.4 | 0.2086 | 284.9 | 0.4341 | 286.2 | 0.0558 | 285.8 | 0.3014 |

solutions containing 0–100 mM chloride. Scanning from open circuit to more positive potentials at 5 mV $s^{-1}$, we observe a concentration-dependent *i–E* profile, where the anodic current increases with increasing chloride concentration. Note in the control experiment (0 mM chloride) that no direct ethanol oxidation occurs in the 0.2–1.3 V *vs.* $Fc^{+/0}$ potential range. And, at an applied bias of 1.0 V *vs.* $Fc^{+/0}$ even at 5 mM chloride, we detect the two-electron 1,1-DEE final product by $^1$H-NMR spectroscopy after a 48 h controlled potential coulometry experiment (Fig. S7, ESI†). Moreover, no chlorinated products are observed, and adding benzene as a radical trap (to form chlorobenzene) product ($^1$H-NMR spectrum in Fig. S8, ESI†) supports that there are no solution-phase active chlorine radicals.

Next, we carried out a variable scan-rate CV (Fig. S9, ESI†) that shows a single onset of current over the range of 25–1000 mV $s^{-1}$ scan rate with a linear relationship between anodic peak current and $\nu^{1/2}$ for the 10 mM chloride case. Together, these results are consistent with a diffusion-controlled two-electron reaction in the forward scan (positive bias). However, the subsequent fast chemical reaction with ethanol renders the reaction electrochemically irreversible, noted by the large >1 V separation between the anodic and cathodic waves. These observations are consistent with our $Cl^+$ mechanistic proposal.

To further assess the plausibility of the mechanism in Scheme 1 with an *in situ* technique, we conducted a UV-Vis spectroelectrochemical experiment scanning from 0.6–1.8 V *vs.* $Fc^{+/0}$ in 100 mM $Bu_4NCl$ solution. EtOCl shows a peak absorbance at $\lambda_{max}$ = 237 nm.[28] The single-wavelength kinetics experiment with a slow-scan rate LSV (1 mV $s^{-1}$) in Fig. 4 shows that anodic current is observed at all potentials, but the EtOCl absorption signal does not grow until the potential reaches 0.9 V *vs.* $Fc^{+/0}$.

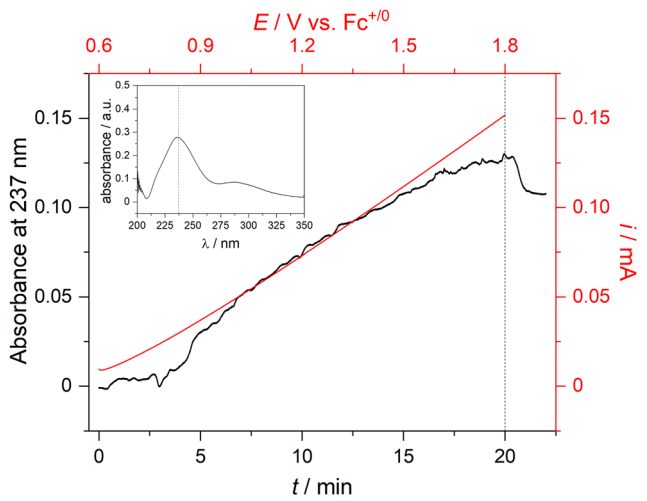


Fig. 4 Spectroelectrochemical identification of EtOCl generation by linear sweep voltammetry in 100 mM $Bu_4NCl$ electrolyte. Electrode: Glassy carbon disk (working), Ag wire (reference), Pt wire (counter). LSV scan rate: 1 mV $s^{-1}$; UV-vis absorption wavelength: 237 nm. The LSV and UV-vis measurement starts at the same time and is designed in such a way that the top and bottom axis are aligned in time. The LSV experiment stops when the time axis reaches 20.0 minutes, and thus a drop is observed in absorption due to the spontaneous degradation of EtOCl.

It continues to grow as the applied potential increases. After the LSV experiment is finished (at 20 min), the signal immediately starts to decrease as EtOCl chemically decays to acetaldehyde and condenses with ethanol to form the 1,1-DEE final product. The absorption spectrum of $Bu_4NCl$ in ethanol is provided for comparison (Fig. S10, ESI†).

## 3. Koutecký–Levich (K–L) analysis of rotating ring-disk electrode data gives the rate constant for the COR in EtOH

Having XPS and LSV data to support that chloride adsorption and oxidation is plausible on GC and gives a two-electron oxidation product, we ask the question what is the rate constant for the COR in ethanol? To measure the kinetics, an RRDE setup was used to assess the rate as a function of chloride-ion concentration, rotation rate ($\omega$), and applied potential. To start, we measured the collection efficiency ($N$) for our RRDE to be 39.9% using the $[Fe(CN)_6]^{3-/4-}$ couple at varying rotation rate (data in Fig. S11, ESI†).

To study a regime from which we can isolate reaction kinetics from mass-transfer effects, we carried out these experiments at 5 mM $Bu_4NCl$ with 100 mM $Bu_4NOTf$ supporting electrolyte to minimize the *iR* drop. Fig. 5a shows the LSV scan in the positive direction from OCP (0.4 V *vs.* $Fc^{+/0}$) on the GC disk electrode with a constant potential held at the ring, −0.4 V *vs.* $Fc^{+/0}$, with varying $\omega$. A control experiment shows that acetaldehyde (the product of EtOCl chemical decomposition) can be reduced at this potential (Fig. S12, ESI†). We note that both the anodic disk current ($i_{disk}$) and the cathodic ring current ($i_{ring}$) increase as $\omega$ increases, and noticeable differences in both the disk and ring currents emerge at potentials greater than 0.8 V *vs.* $Fc^{+/0}$.

To quantify the kinetics of the COR in EtOH as a function of applied potential, we carried out K–L analysis in the potential range 1.00–1.20 V *vs.* $Fc^{+/0}$ with the equation:[29]

$$\frac{1}{i} = \frac{1}{i_k} + \left(\frac{1}{0.62nFAD^{\frac{2}{3}}\nu^{-\frac{1}{6}}C}\right)\omega^{-\frac{1}{2}} \quad (4)$$

where $i$ is the measured current, $i_k$ is the kinetic current, $n$ is the number of electrons transferred, $F$ is Faraday's constant (96 485 C $mol^{-1}$), $A$ is the GC disk electrode surface area (0.126 $cm^2$), $D$ is the diffusion coefficient of chloride in EtOH ($1.52 \times 10^{-6}$ $cm^2$ $s^{-1}$), determined from applying the Cottrell equation to a constant potential chronoamperometry (CPC) measurement (Fig. S13, ESI†) in which current is measured in a quiescent solution,[30] $\nu$ is the kinematic viscosity of EtOH ($1.391 \times 10^{-2}$ $cm^2$ $s^{-1}$),[31] $C$ is the bulk concentration of the chloride, $5 \times 10^{-6}$ mol $cm^{-3}$ and $\omega$ is the rotation rate of the electrode (rad $s^{-1}$). Fig. 5b shows the K–L plots of $i^{-1}$ *vs.* $\omega^{-1/2}$. We observe the expected linear increase, indicating the ideal RDE response, and $i_k$ (determined from the *y*-intercept) for the COR varies from 242 μA (1.0 V) to 589 μA (1.2 V). From the slopes, $n$ is 1.65, consistent with two-electron oxidation of $Cl^-$ to EtOCl.

Given $i_k$, we then can determine the kinetic rate constant for the forward reaction to form EtOCl, $k_f$, given by the equation:[29]

$$i_k = k_f nFAC^m \quad (5)$$

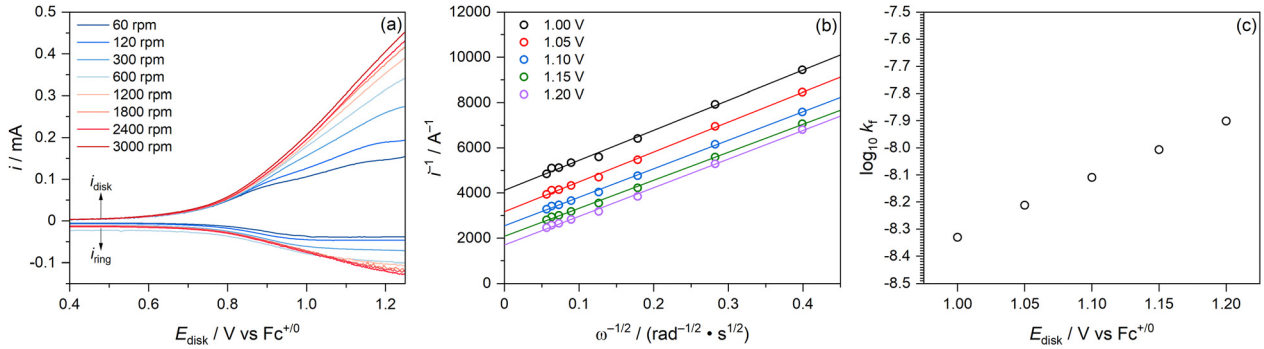


Fig. 5 (a) RRDE LSV ($i$–$E_{disk}$) with a GC disk and Pt ring in 5 mM $Bu_4NCl$ and 100 mM $Bu_4NOTf$ electrolyte in EtOH solvent. The scan rate is 20 mV $s^{-1}$ and $E_{ring}$ is poised at −0.4 V *vs.* $Fc^{+/0}$. The cell is sparged with argon prior to recording the data; (b) K–L plot of the LSV data; (c) trend in kinetic rate constant determined from the kinetic current as a function of disk potential.

where $m$ is the apparent reaction order, determined by a separate analysis of $i_{disk}$ as a function of chloride concentration at a constant $\omega$ (Fig. S14 and Table S1, ESI†). Fig. 5c shows the trend of kinetic rate constant for the COR in ethanol, presented as $\log_{10}(k_f)$ *vs.* $E_{disk}$. Rate constants for both the electrochemical COR step ($\sim 10^{-8}$ cm $s^{-1}$) and the chemical EtOCl decomposition step ($7 \times 10^{-4}$ $s^{-1}$) from this work and a previous study, respectively, quantify the rate of chloride-mediated ethanol oxidation on a GC electrode.[15] From the control experiment data in Fig. S15 (ESI†), the rate constant for direct ethanol oxidation (at unit activity) at 1.6 V *vs.* $Fc^{+/0}$, a kinetically-limited regime for that reaction, is $10^{-13}$ cm $s^{-1}$, some five orders of magnitude slower than the COR in ethanol.

Considering the ring current, we compare the apparent collection efficiency, $N_{app}$ during the COR experiment to that measured using the $[Fe(CN)_6]^{3-/4-}$ couple (Fig. S11, ESI†). We find excellent agreement between the two values, with $N_{app}$ = 39%, in agreement with fast decay to acetaldehyde, which reacts at the ring.

## Conclusions

A combination of electrochemical techniques, including CV and LSV of chloride solutions using quiescent solutions and RRDEs provide evidence of a clean two-electron mechanism for chloride oxidation on a GC disk electrode to form EtOCl. XPS analysis corroborates the adsorption of both chloride and ethanol on GC. Koutecký–Levich analysis shows that the $k_f$ for the COR in ethanol is $10^{-8}$ cm $s^{-1}$ at potentials for which direct ethanol oxidation does not occur, and spectroelectrochemical measurements show one sole chloride oxidation product, EtOCl. This work establishes a plausible mechanism for electrochemical chloride-mediated ethanol oxidation, and future work includes probing other primary alcohol substrates and using other halide/oxyhalide anion redox couples to test changes in kinetics as well as the generality of this mechanism.

## Author contributions

R. D. V. D. contributed through, investigation, visualization of the data through graphics, formal analysis (LSV, CV, XPS, CPC, $^1$H-NMR, and spectroelectrochemical data) and writing, reviewing, and editing the revised manuscript. S. L. contributed through conceptualization of the work, investigation, and formal analysis (LSV, RRDE and spectroelectrochemical data), visualization of data through graphics, as well as writing the original draft. K. H. M. contributed through investigation (CV and RRDE data). B. M. B. contributed through funding acquisition, supervision, and writing – review & editing.

## Data availability

The data supporting this article have been included as part of the ESI.†

## Conflicts of interest

There are no conflicts to declare.

## Acknowledgements

This research was supported by a grant from the U.S. Department of Energy, Basic Energy Sciences, Catalysis Science Program, under Award No. DE-SC0006587. The authors acknowledge the financial support of the University of Michigan College of Engineering and NSF grant #DMR-0420785 (Kratos Axis Ultra XPS), and technical support from the Michigan Center for Materials Characterization.

## Notes and references

1 B. You and Y. Sun, *Acc. Chem. Res.*, 2018, **51**, 1571.
2 S. Ardo, D. F. Rivas, M. A. Modestino, V. S. Greiving, F. F. Abdi, E. A. Llado, V. Artero, K. Ayers, C. Battaglia, J. P. Becker and D. Bederak, *Energy Environ. Sci.*, 2018, **11**, 2768.
3 J. Chen, C. Dong, H. Idriss, O. F. Mohammed and O. M. Bakr, *Adv. Energy Mater.*, 2020, **10**, 1902433.
4 R. K. Prasad, S. Chatterjee, P. B. Mazumder, S. K. Gupta, S. Sharma, M. G. Vairale, S. Datta, S. K. Dwivedi and D. K. Gupta, *Chemosphere*, 2019, **231**, 588.
5 Y. Holade, H. Guesmi, J. S. Filhol, Q. Wang, T. Pham, J. Rabah, E. Maisonhaute, V. Bonniol, K. Servat, S. Tingry,

D. Cornu, K. B. Kokoh, T. W. Napporn and S. D. Minteer, *ACS Catal.*, 2022, **12**, 12563.
6 O. Rosales-Calderon and V. Arantes, *Biotechnol. Biofuels*, 2019, **12**, 1.
7 L. Yaqoob, T. Noor and N. Iqbal, *RSC Adv.*, 2021, **11**, 16768.
8 T. A. Ivandini, T. N. Rao, A. Fujishima and Y. Einaga, *Anal. Chem.*, 2006, **78**, 3467.
9 D. M. Heard and A. J. Lennox, *Angew. Chem., Int. Ed.*, 2020, **59**, 18866.
10 A. Badalyan and S. S. Stahl, *Nature*, 2016, **535**, 406.
11 R. Ciriminna, G. Palmisano and M. Pagliaro, *ChemCatChem*, 2015, **7**, 552.
12 A. G. Breuhaus-Alvarez, S. Li, N. Z. Hardin and B. M. Bartlett, *J. Phys. Chem. C*, 2021, **125**, 26307.
13 J. L. DiMeglio, A. G. Breuhaus-Alvarez, S. Li and B. M. Bartlett, *ACS Catal.*, 2019, **9**, 5732.
14 J. L. DiMeglio, B. D. Terry, A. G. Breuhaus-Alvarez, M. J. Whalen and B. M. Bartlett, *J. Phys. Chem. C*, 2021, **125**, 8148.
15 S. Li and B. M. Bartlett, *J. Am. Chem. Soc.*, 2021, **143**, 15907.
16 F. D. Chattaway and O. G. Backeberg, *J. Chem. Soc., Trans.*, 1923, **123**, 2999.
17 R. R. Gagne and D. N. Marks, *Inorg. Chem.*, 1984, **23**, 65.
18 D. Serra, M. C. Correia and L. McElwee-White, *Organometallics*, 2011, **30**, 5568.
19 S. Choi, W. I. Choi, J. S. Lee, C. H. Lee, M. Balamurugan, D. Schwarz, Z. S. Choi, H. Randriamahazaka and K. T. Nam, *Adv. Mater.*, 2023, 2300429.
20 Y. Wang, Y. Liu, D. Wiley, S. Zhao and Z. Tang, *J. Mater. Chem. A*, 2021, **9**, 18974.
21 C. Lucky, T. Wang and M. Schreier, *ACS Energy Lett.*, 2022, **7**, 1316.
22 B. V. Tilak, *J. Electrochem. Soc.*, 1979, **126**(8), 1343.
23 P. Chen and R. McCreery, *Anal. Chem.*, 1996, **68**, 22.
24 J. F. Moulder, Handbook of X-ray Photoelectron Spectroscopy, *Phys. Electron.*, 1995, 62.
25 J. R. Araujo, B. S. Archanjo and K. R. de Souza, *et al.*, *Biol. Fertil. Soils*, 2014, **50**, 1223–1232.
26 J. F. Moulder, Handbook of X-ray Photoelectron Spectroscopy, *Phys. Electron.*, 1995, 63.
27 F. C. Loh, K. L. Tan and E. T. Kang, *Eur. Polym. J.*, 1991, **27**, 10.
28 T. P. Jungkamp, U. Kirchner, M. Schmidt and R. N. Schindler, *J. Photochem. Photobiol., A*, 1995, **91**, 1.
29 A. J. Bard and L. R. Faulkner, Methods Involving Forced Convection - Hydrodynamic Methods, *Electrochemical Methods: Fundamentals and Applications*, John Wiley & Sons, 2nd edn, 2001, pp. 331–367.
30 I. Ruff, V. J. Friedrich, K. Demeter and K. Csillag, *J. Phys. Chem.*, 1971, **75**, 3303–3309.
31 A. N. Petrov and G. A. Alper, *Zh. Obshch. Khim.*, 1992, **62**, 1231.

 